CERN – EUROPEAN ORGANIZATION FOR NUCLEAR RESEARCH

CLIC – Note – 1066

NEW CLIC-G STRUCTURE DESIGN

Hao ZHA, Alexej GRUDIEV
European Organization for Nuclear Research, Geneva, Switzerland

Geneva, Switzerland
11th May 2016

CLIC-G*: A new RF design of the CLIC main linac accelerating structure towards higher gradient at lower cost.

Hao Zha, Alexej Grudiev

1. Introduction

The baseline design of the Compact Linear Collider main linac accelerating structure is called ‘CLIC-G’. It is described in the CLIC Conceptual Design Report (CDR) [1]. As shown in Fig. 1, a regular cell of the structure has four waveguides to damp unwanted high-order-modes (HOMs). These waveguides are dimensioned to cut off the fundamental working frequency in order to prevent the degradation of the fundamental mode Q-factor. The cell geometry and HOM damping loads had been extensively optimized in order to maximize the RF-to-beam efficiency, to minimize the cost, and to meet the beam dynamics and the high gradient RF constraints [2].

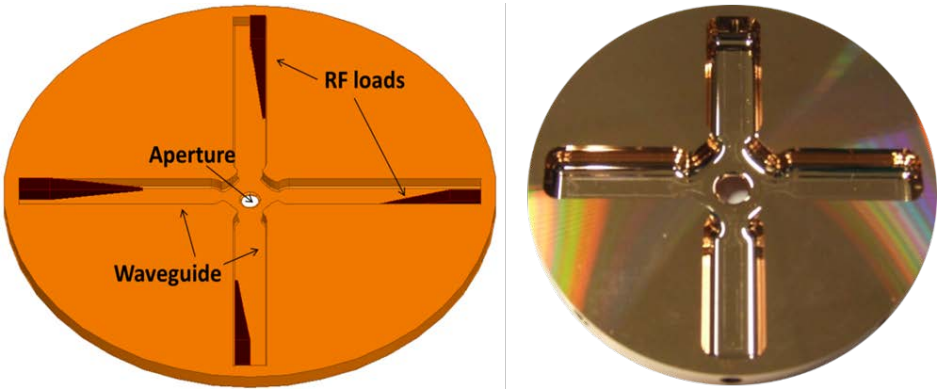

Figure 1: CLIC base line accelerating structure cell.

Due to the importance of the long-range transverse wakefield suppression in the CLIC main linac, an experimental verification in this aspect of the CLIC-G design had been carried out in the FACET facility [3]. As shown in Fig. 2, two beam lines were used to deliver both positron and electron beams in a 1.5 m length of six CLIC-G structure prototypes. The positron beam passed thought the CLIC-G structure with a given transverse offset in order to excite the dipolar higher-order-mode wakefield. The electron beam was deflected by the wakefield and its trajectory was measured by downstream BPMs.

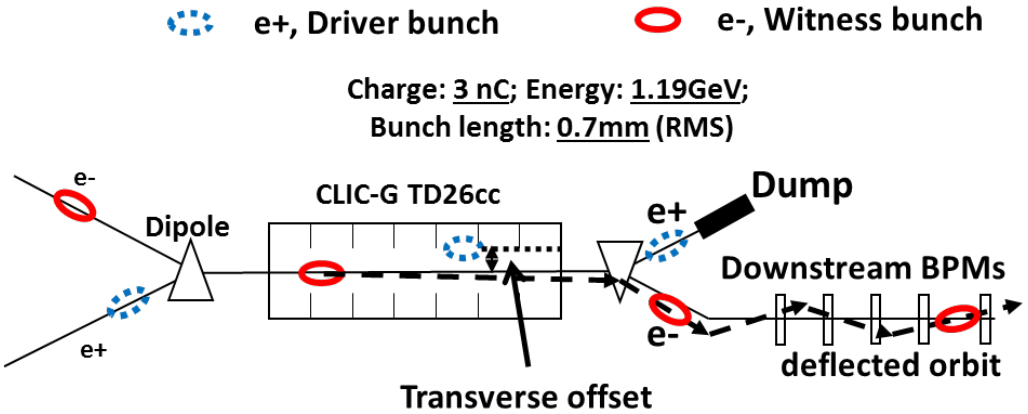

Figure 2: Wakefield measurement of CLIC accelerating structure on the FACET facility.

The wakefield value was deduced from the deflected electron beam trajectory . Fig. 3 shows the measured results together with GDFIDL simulations on the same structure [4]. The transverse wakefield measured at the position of the second bunch was 5 V/pC/m/mm, which verified the long-range wakefield suppression of the CLIC-G design. The excellent agreement between simulation and measurements as demonstrated in the plots gives us confidence in the accuracy of the wakefield simulation codes. This is important for the design work

described below where all improvements made on the structure and HOM damping load design are based on simulations.

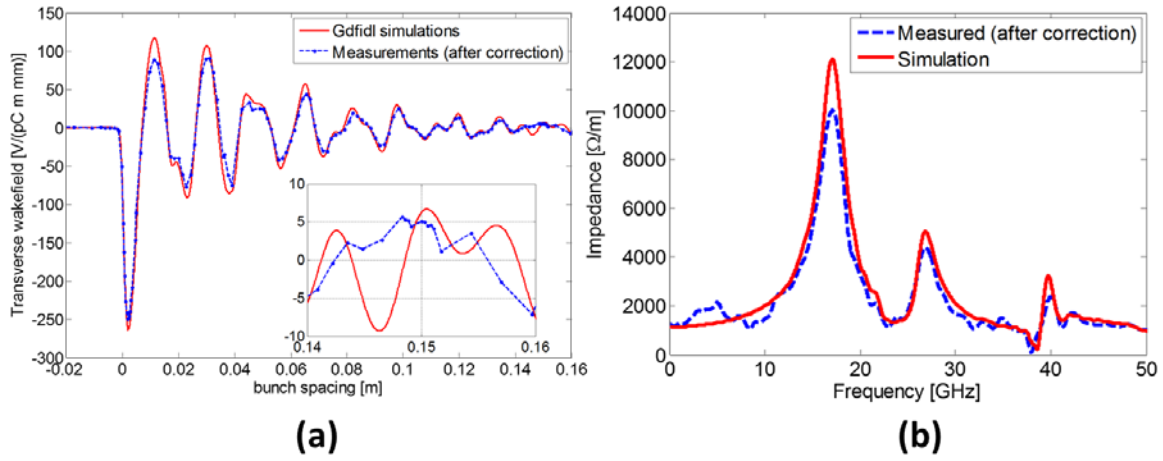

Figure 3: Wakefield measurements results (a): time-domain transverse wakefield; (b): wakefield spectrum.

High power tests of CLIC structures have been underway at several test stands at CERN and KEK [5-10]. The results are summarized in Fig. 4 [11]. Recent tests show that the unloaded gradient achieved in the CLIC-G prototype structure for the CLIC effective pulse length (180 ns) and required break down rate ($3*10^{-7}$) is 96 MV/m. The corresponding loaded gradient would be about 80 MV/m. The highest gradient demonstrated so far is 120 MV/m which was achieved in an undamped structure with 24 cells with an iris geometry identical to the CLIC-G. Generally speaking, the gradient achieved in damped CLIC structures were lower than that of undamped ones. One possible explanation is that he pulse surface temperature rise of the damped structures are 40-50 K, two times higher than that of undamped structure.

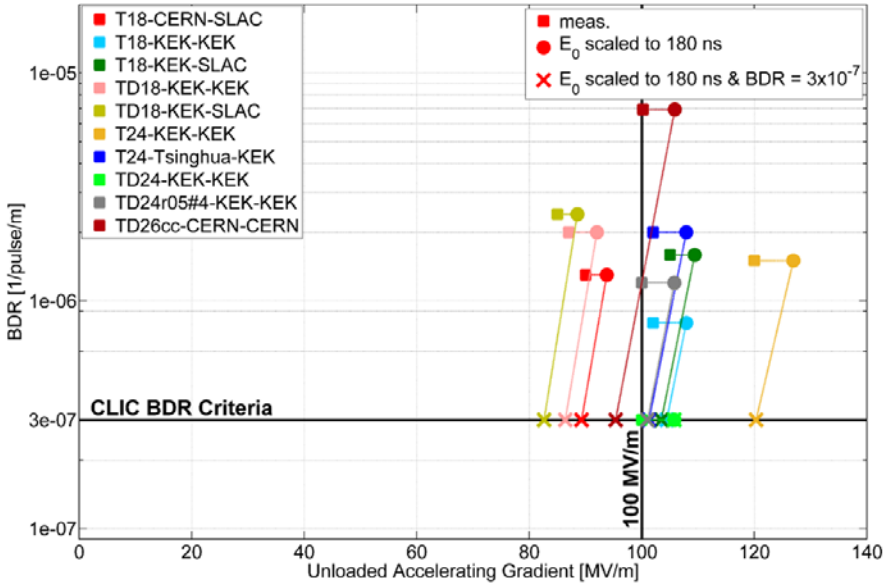

Figure 4: High power tests on CLIC accelerating structure prototypes [11].

Assessment of the machining cost of the CLIC-G structure was also studied [12]. The cost model shows that the structure cell with a larger rounding will significantly reduce the cost. Changing the rounding in the geometry will also have the impact on the structure design in the aspect of surface field and wakefield suppression, which results in a new structure design. This study, together with the high power tests for the CLIC-G structure, had raised the need of re-optimizing the structure geometry to minimize the machining cost and the surface magnetic field.

2. New wall geometry of waveguide damped cells

Pulsed surface heating in the accelerating structure is one of the main limitations for accelerating gradient. As shown in Fig. 5, the waveguide damped cell (middle cell of the baseline design) has higher magnetic field than that of undamped cell with same iris geometry. The high magnetic field of the waveguide damped cell is concentrated at the cell wall, of which the profile is an elliptical arc in CLIC-G. The elliptical wall geometry had been optimized to have a very flatten magnetic field distribution along the wall profile line to avoid hot spot on the wall. However, two bumps can still be seen from the plot. The enhancement of magnetic field at the two bumps is due to the mutation of curvature in the profile line, as seen in Fig. 6 (b).

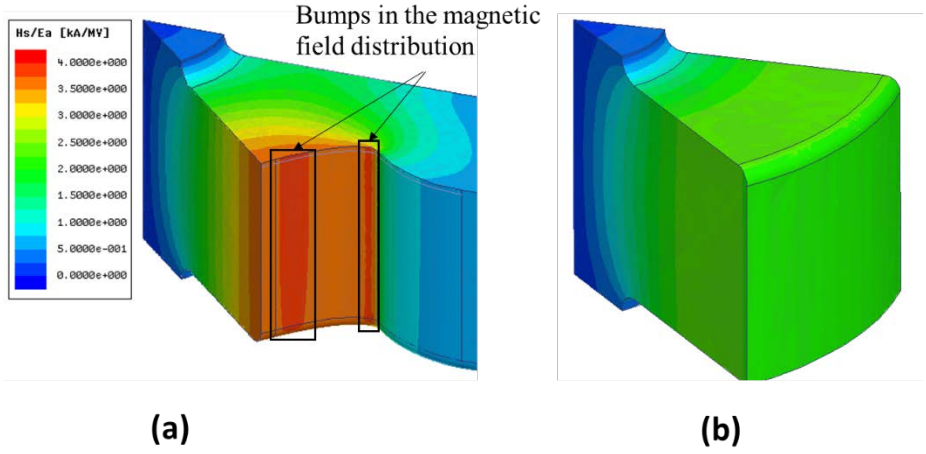

Figure 5: Magnetic field distribution in the middle cell of CLIC base line accelerating structure (a) compared with an undamped cell (b).

The wall geometry could be improved and the bumps removed from the field distribution. A 4-th order polynomial function based profile was proposed, as shown in Fig. 6 (a). Compared to the elliptical wall profile, the polynomial has a smoother curvature change. The magnetic field distribution of both wall profiles for middle cell of the base line design were simulated by HFSS and are plotted in Fig. 7. The polynomial function based design decreases the maximum magnetic field by 2%, which corresponds ~2 K temperature reduction to the pulse surface heating.

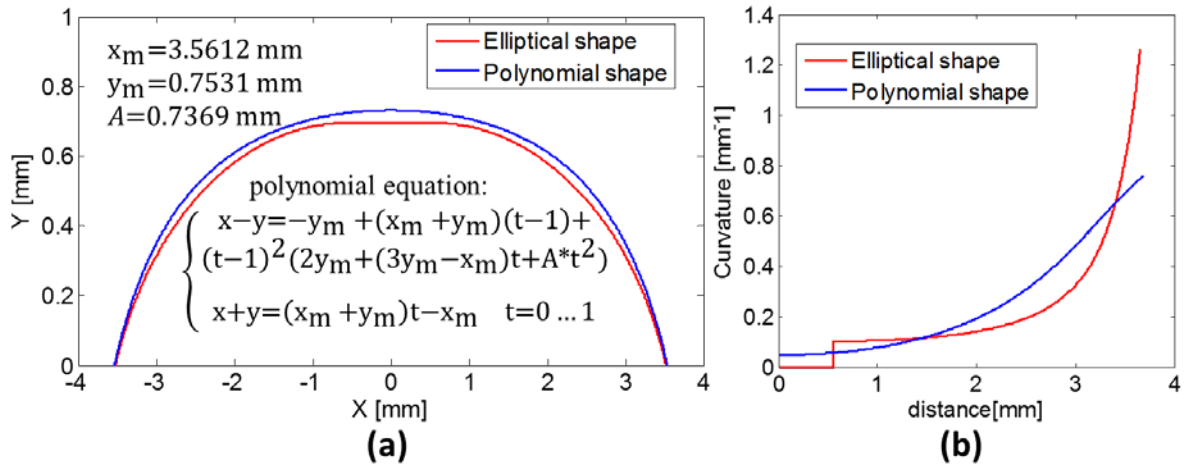

Figure 6: Shape (a) and curvature (b) of base line elliptical wall profile and new proposed polynomial profile.

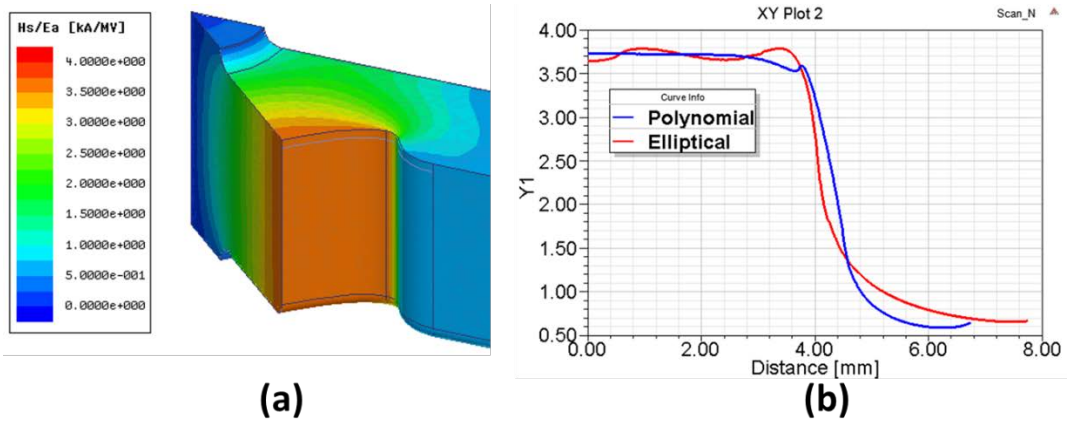

Figure 7: Magnetic field distribution in the middle cell of CLIC accelerating structure with new proposed polynomial profile

3. Optimization on the rounding and waveguide geometries

Milling is the main process in the machining of CLIC accelerating structures. An arc shape is usually employed in the milling head cutter in order to avoid sharp edge and protect the cutter. During the milling process, the cutter leaves arc-shape ridges on the metal surface which introduce roughness on the structure surface (as seen in Fig. 8). The height of the ridge is determined by the milling step and the radius of the arc shape in the milling cutter, as expressed in formula in the Fig. 8. A small cutter radius requires a finer milling interval which consumes more machining time and cost, in order to meet the same surface roughness specifications.

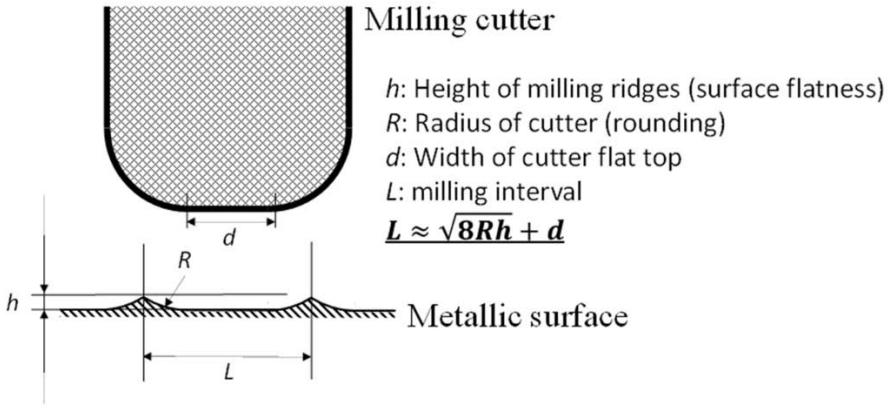

Figure 8: Surface flatness and rounding in the milling process

The cutter radius is limited by the minimum rounding in the structure. Thus increasing the rounding of the cell structure can reduce the machining cost. However, the larger rounding reduces the cross-section area of the waveguide and consequently the coupling of the HOM fields into the waveguides. In this case, damping waveguides with larger width and opening are needed for structure cells to maintain same wakefield suppression. However, increasing waveguide dimensions results in a higher surface magnetic field. Thus, a comprehensive study was necessary for the selection of the rounding.

Among all the geometrical parameters (rounding radius, waveguide width and waveguide opening) related to the rounding study, the width of waveguide opening had the most significant impact on both the wakefield suppression and the surface magnetic field. The strategy in the optimization was to first determine the waveguide opening for different rounding and waveguide widths. When the waveguide opening is larger, the wakefield suppression goes stronger and the surface magnetic field goes higher. In order to minimize the surface magnetic field, the value of waveguide opening was as small as to keep the wakefield suppression

same level as the baseline CLIC-G design, which are given by GDFIDL simulations of the long-range transverse wakefield in the tapered CLIC-G structure. With these minimum waveguide openings, HFSS simulations of the CLIC-G middle cell with different rounding and waveguide widths were carried out. The plot of maximum surface magnetic field versus rounding and waveguide width are shown in Fig. 9 (a). As seen in the plots, the optimum waveguide width is around 10 – 10.3 mm for all roundings.

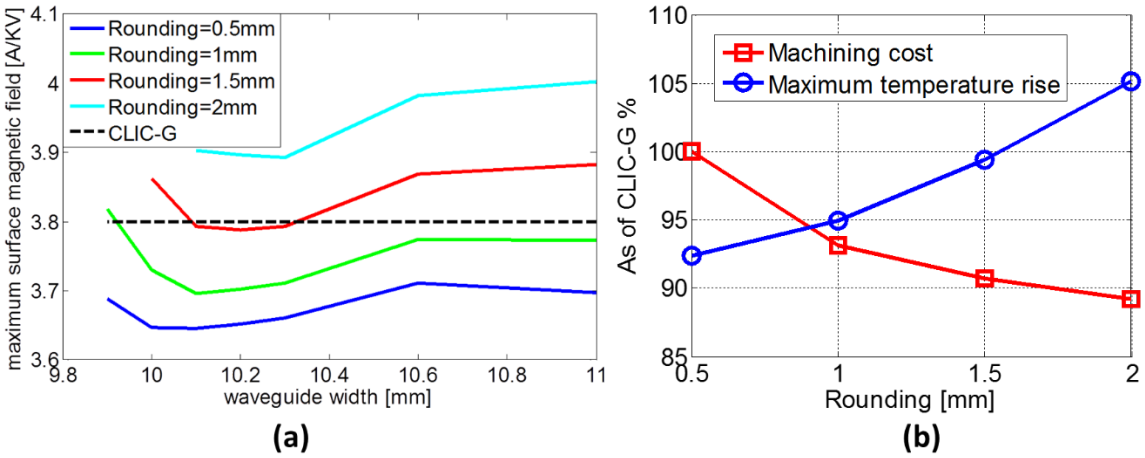

Figure 9: Plot of maximum magnetic field versus rounding and waveguide width (a) and plot of machining cost and pulsed surface heating versus rounding (b).

A plot of machining cost reduction and reduction of the pulsed surface heating temperature rise versus rounding is shown in Fig. 9 (b). The temperature rise was calculated from the solutions with optimum waveguide width. Due to the optimization of the wall profile and waveguide width, the temperature rise of the solution with 0.5 mm rounding is lower than that of CLIC-G, leaving margin to increase the rounding. We chose the 1 mm rounding design (correspond optimum waveguide width: 10.1 mm) for its significant reduction both on cost and temperature rise. A larger rounding was not considered because the further improvement on cost is small and the temperature increase is higher.

4. Full tapered structure design

The baseline CLIC-G design has 26 regular cells and 2 compact coupler cells as shown in Fig. 10 (a). The iris apertures in the design range from 3.15 mm to 2.35 mm. The average value and tapering of the iris aperture was determined by the global optimization which considered the performance and the total cost. The iris profiles have been optimized to minimize the surface electric field and the modified Poynting vector *Sc* [13]. This iris geometry is already well designed and will not be changed in the new design.

The optimizations introduced in Sec. 2 and Sec. 3 were for the middle cell of the CLIC structure. These optimizations should be extended to all other cells in order to get the full tapered structure design. Dimensions in the wall profile were individually optimized for each cell to get flatten distributions of magnetic field. The optimization of rounding (1 mm), waveguide width (10.1 mm) and waveguide openings (8.14 mm) were the same for all the cells.

In the baseline CLIC-G design, the upstream cell has the highest point for the pulse temperature rises, as seen in Ref [2]. Due to the dependency of waveguide opening width on the surface magnetic field, the temperature rise of upstream cells could be decreased by reducing the waveguide openings. Meanwhile, the waveguide openings of downstream cells were increased to compensate the weaken of wakefield suppression in upstream cells. Fig. 11 shows the tapering on the waveguide openings versus the change of temperature rises. A quadratic function based tapering on the waveguide openings was selected and the maximum temperature rise decreases by 2 K.

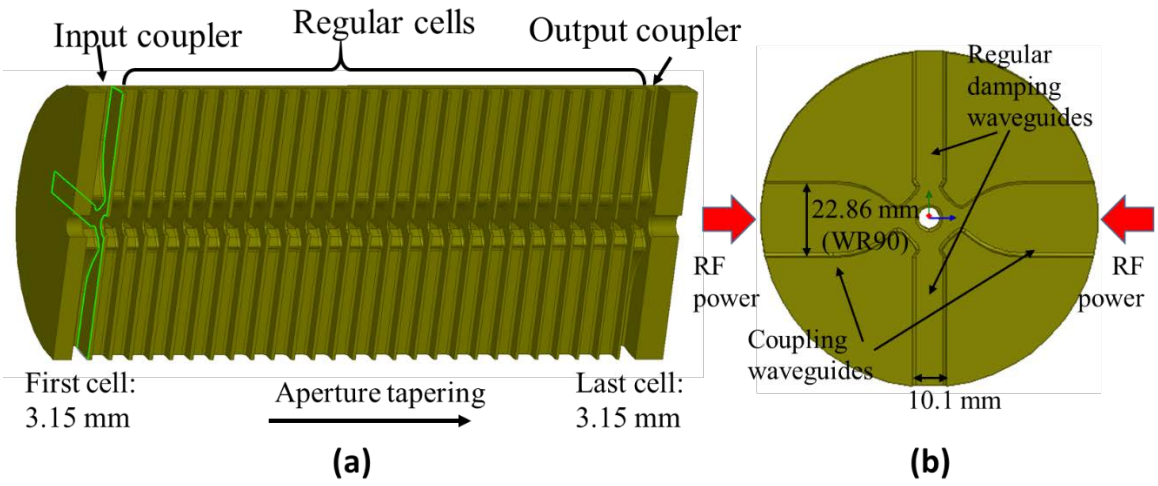

Figure 10: (a) Sketch of CLIC accelerating structure; (b) Geometry of compact coupler cell.

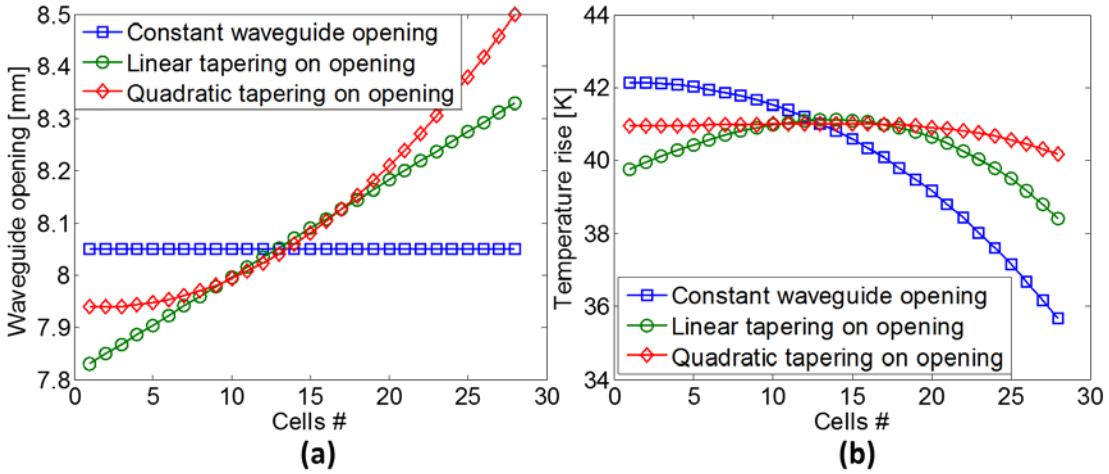

Figure 11: Tapering on waveguide openings.

The geometry of compact input and output couplers in the new CLIC-G design is similar to the baseline CLIC-G design. As shown in Fig. 10(b), two of the waveguide branches (damping waveguides) in coupler cells use same geometry as that of nearest regular cell: dimensions of damping waveguides in the input coupler cell were taken from the first regular cell; and dimensions of the output cell were from the last regular cell. The other two waveguide branches (coupling waveguides) in coupler cells have larger waveguide widths (WR90 dimension) in order to transmit the fundamental RF power.

The dimensions of the waveguide openings in the coupling waveguides are adjusted to match the coupling from WR90 waveguides to structure cells. The design procedure was to match the output coupler first, otherwise the reflection at the output coupler will disturb the tuning and matching the upstream of the structure includings the input coupler. Reflection due to the mismatch in the output coupler will cause a standing wave component in the electrical field distribution of structure cells. As seen in Fig. 12 (a), the backward reflection at the output coupler is not same as the port reflection co-efficiency S_{22} due to both the structure tapering and the finite conductivity of structure wall. This backward reflection could be only calculated by the amplitude of frontward and backward wave analysed from the field distribution of downstream cells, as expressed in below equation:

$$\left.\begin{array}{c} E_1 = a + b \\ E_2 = ae^{j\varphi} + be^{-j\varphi} \\ E_3 = ae^{2j\varphi} + be^{-2j\varphi} \end{array}\right\} \rightarrow \text{Reflection} = \frac{b}{a} = \frac{\sqrt{u^2-4}-v}{\sqrt{u^2-4}+v}, u = \frac{E_3+E_1}{E_2}, v = \frac{E_3-E_1}{E_2} \quad (1)$$

where E_1, E_2 and E_3 are the peak electrical field (complex number) of last three cells, a and b are the amplitudes of forward-wave and backward-wave as seen in Fig. 12 (a), φ are the phase advance (2/3π) between two cells. The reflection due to the mismatch in the input coupler could be directly exanimated by the port reflection co-efficiency S_{11} in the coupling waveguides if downstream of the structure is good matched. Dimensions of both output and input coupler cells were carefully tuned in HFSS simulations and the reflection of input coupler is less than -50 dB as seen in Fig. 12 (b). According to equation (1), the backward reflection at the output coupler was calculated by field distribution shown in Fig .13 and is also less than -50 dB. Fig 13 shows a flat field distribution which indicates that the structure geometry is already well tuned.

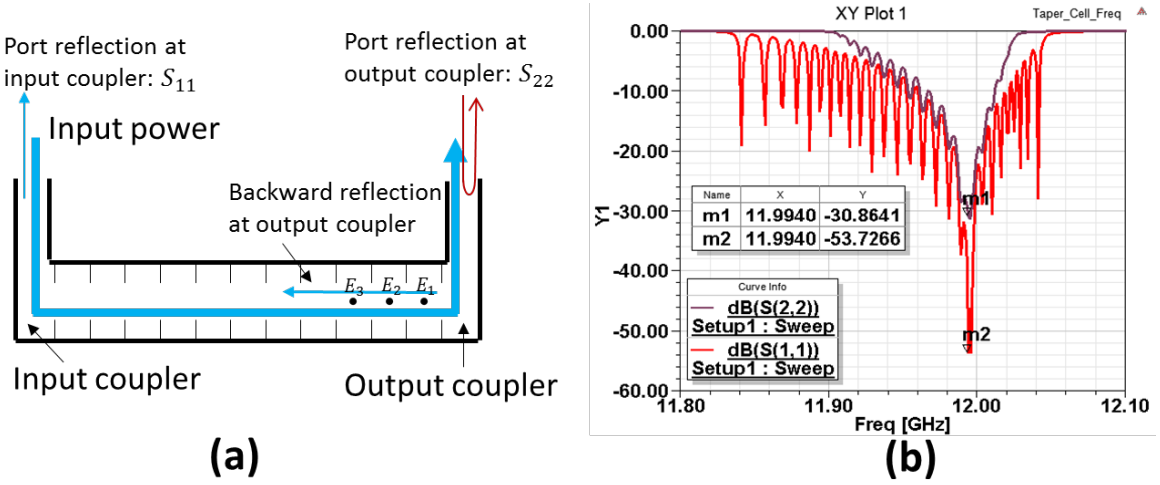

Figure 12: (a) Reflection co-efficiencies in a travelling wave structure; (b) Port-reflection of new CLIC-G tapered structure (HFSS simulations).

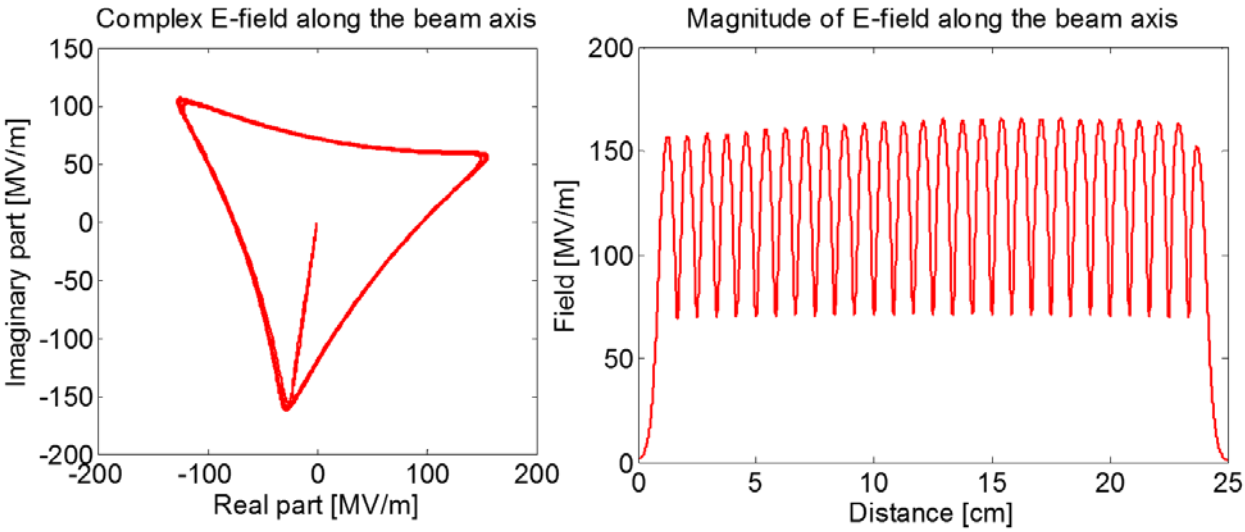

Figure 13: Electrical field distribution on the beam axis of the new CLIC-G tapered structure.

The newly optimized design integrates all the features introduced above and was named 'CLIC-G*'. The serial alphabet 'G' keeps same since the new design doesn't change the iris parameters. The detailed parameters are listed in Table 1. Compared to CLIC-G, this new design reduces the temperature rise by 20% from 52 K to 41 K. The estimated cost is reduced by 7% and the power consumption is 1MW lower due to

higher shunt impedance of structure cells. The simulated wakefield of the new design is shown in Fig. 14 and is compared to the CLIC-G design from the CDR. The attenuation of two curves are similar to each other. The wakefield potential of the new design at the positon of the second bunch (0.15 m) is 2 V/pC/m/mm, as required by beam dynamics.

Tab. 1: Structure Parameters of CLIC-G* design. The parameters of CLIC-G inside the braces are given in [2], outside are recalculated in latest HFSS version.

	CLIC-G	CLIC-G*
Rounding[mm]	0.5	1.0
Manufacturing cost reduction	--	7%
Shunt impedance [MΩ/m]	92.0	95.4
Peak input power [MW]	63.4	62.4
RF to beam efficiency	27.9%	28.4%
Filling time [ns]	67	66
Maximum electric field [MV/m]	248(230)	250
Maximum *Sc* [MW/mm^2]	5.70	5.65
Maximum temperature rise [K]	52(47)	41

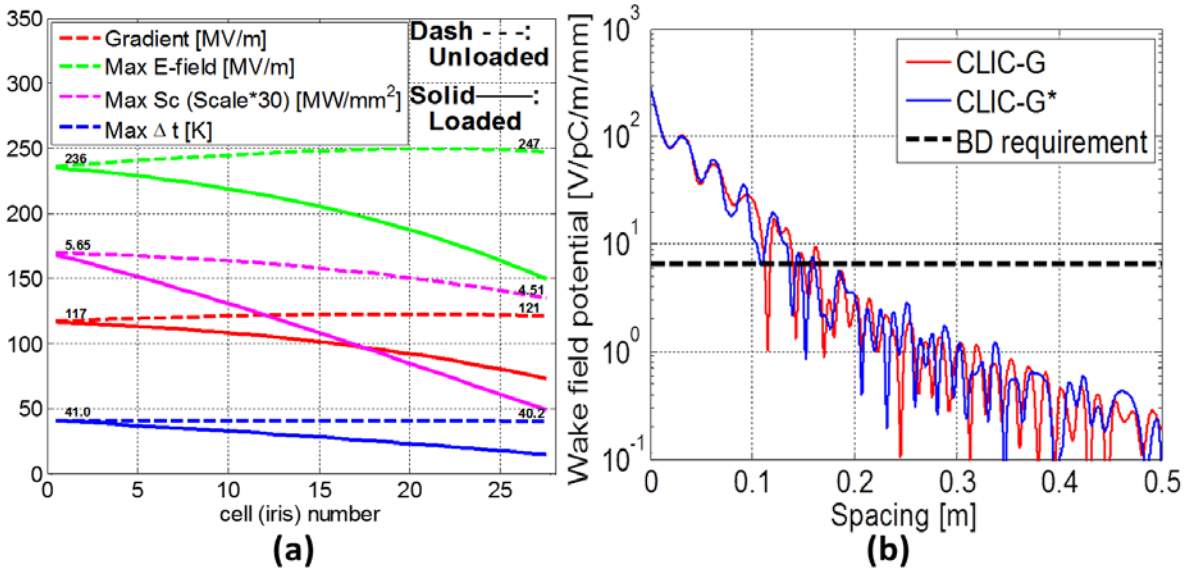

Figure 14: (a) Distribution of RF parameters (red: accelerating gradient, blue: pulse temperature rise, green: maximum surface electrical-field, magenta: maximum modified pointing vector [13]) along the CLIC-G* structure cells; (b) Simulation results of transverse wakefield in the old baseline CLIC-G and new CLIC-G* structures.

5. HOM load design

Beam dynamics study for the CLIC main linac indicate that that the transverse wakefield kick of a bunch on the following bunch must be suppressed to less than 6.6 V/pC/m/mm, in order to maintain the beam stability in the main linac. The peak value of the excited transverse wakefield is about 250 V/pC/m/mm. Therefore the wakefield kick should be suppressed by nearly two-orders of magnitude between one bunch separation (0.5 ns). In order to meet this criteria, HOM loads in the structure cells should provide strong absorption to all major dipole modes with their frequencies ranged from 15 GHz to 45 GHz. The design of

HOM loads was verified by the GDFIDL simulations on a CLIC-G* structure assembled together with the HOM loads.

A silicon carbide material named “EkaSiC-P” is used as a reference for the design of load. The measured data of the permittivity and the loss tangent of “EkaSiC-P” are shown in Fig. 15 (a) [14]. Parameterized data on the permittivity and the dielectric loss tangent for this material in the GDFIDL simulations are also shown. The geometry of the HOM loads was designed as a smooth tapered box as shown in Fig. 15 (b). The tip in the geometry has small cross-section area in order to reduce the reflection from the tip and the design of smooth tapered section is to achieve strong and broad-band absorption.

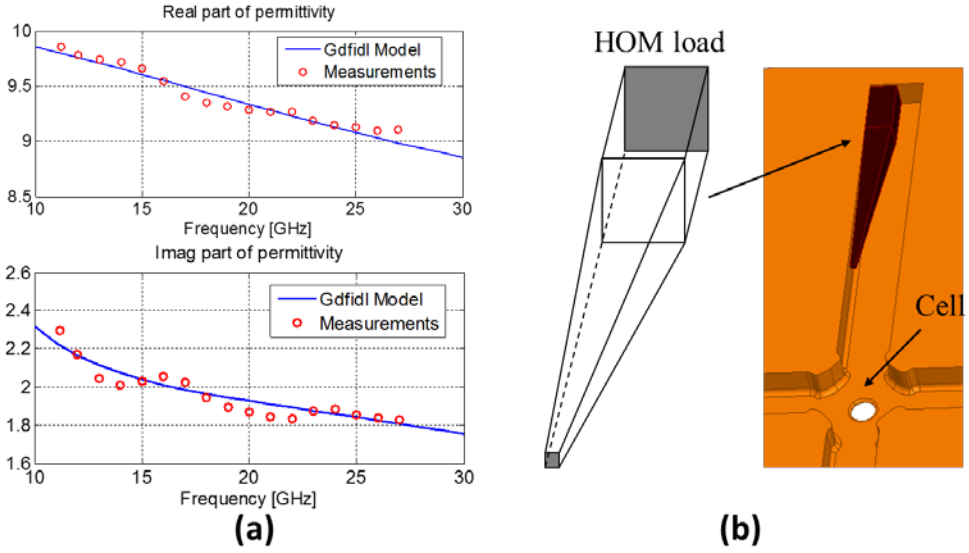

Figure 15: Material properties (a) and geometry (b) of the HOM load.

HOM loads are placed in the damping waveguides of the CLIC accelerating structure cell. Though the frequency of fundamental working mode is under cut off in the waveguides, there is still a small fraction of the fundamental mode RF power penetrating in the waveguide and which is then absorbed by HOM loads. Since the field of the working mode is exponentially decaying versus the depth in the waveguide, a certain distance from the load to the central cavity is needed to reduce power dissipation in the HOM loads as shown in Fig. 16 (a). In the baseline CLIC-G design, this distance is 5 cm and length of the HOM load is 4 cm, as shown in Fig. 16 (b). The overall cell diameter is 20 cm. Estimated absorb power of working mode at one HOM load is about 50 W. If running at 50 Hz repetition rate and 240 ns pulse width, the average power dissipation at one HOM load is 0.6 mW.

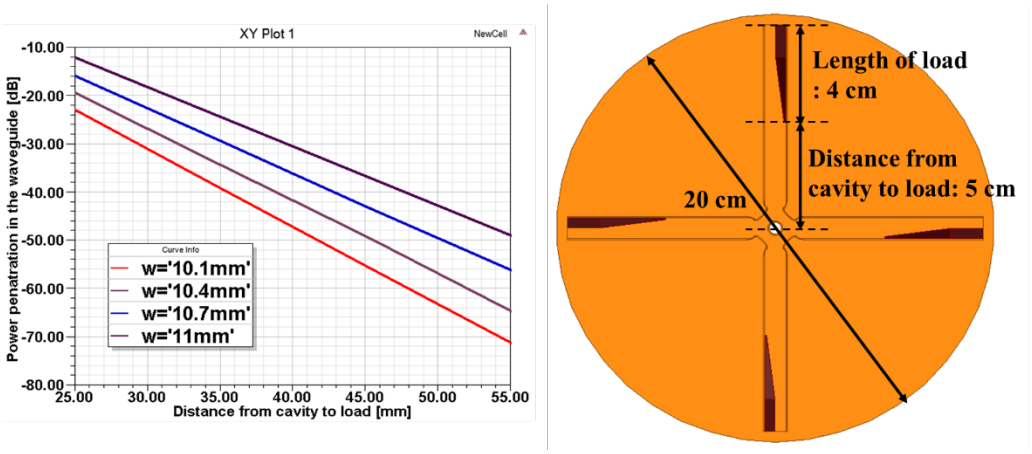

Figure 16: Power dissipation in the HOM load of working frequency versus the distance from the cavity central to the load.

The new CLIC accelerating structure design has a narrower waveguide width (10.1 mm) than the baseline design (11 mm). The distance between the HOM load and the cavity of the new design can be shorter since the decay of working mode is stronger. The geometry of the HOM load is re-optimized to fit the beam dynamic requirements. As shown in Fig. 17 (a), the length of the HOM load for the new design is 4.4 cm, a bit longer than the base line design. This is because that length of smooth tapered section needs to be matched with the propagating wavelength of the HOM, which becomes longer for a smaller waveguide width. The overall cell diameter of the new design is still smaller (17 cm) since the distance from the cavity to the HOM load is shorter (3.1 cm). Wakefield simulation results of the new structure and HOM load design is shown in Fig. 17 (b) and compared to results of base line design. Tab. 2 lists three transverse beam jitter amplification factors: F_c, F_{rms} and F_{worst}, which describe the amplification of transverse beam jitter in the main linac due to the long range transverse wakefield [15]. These factors represent effects of long-range wakefield on the beam instability. Given by the numbers listed in Tab. 2, the new CLIC structure and correspond HOM load design shows better wakefield suppression than that of the base line design.

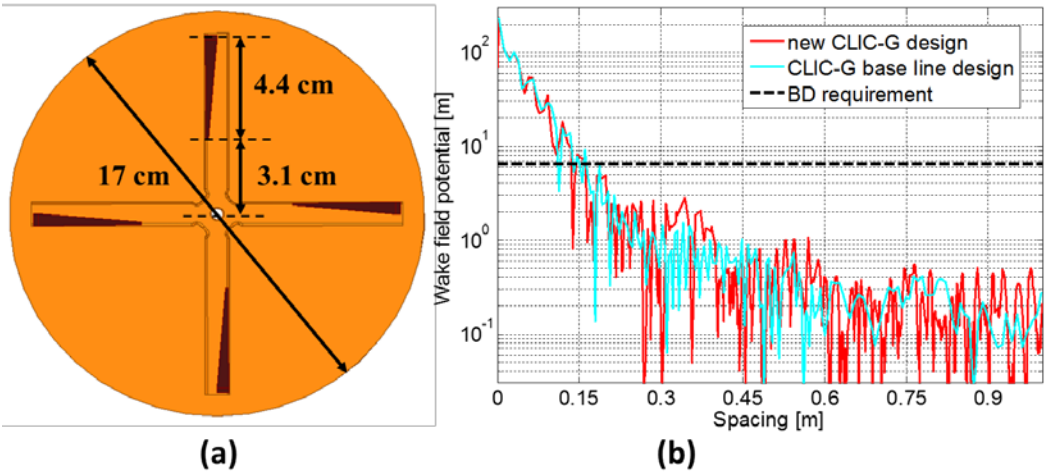

Figure 17: Geometry (a) and wakefield results (b) of the HOM load design for CLIC-G* structure with regular damping wavegudes

The new structure design has a 17 cm cell diameter, which is still rather large for manufacturing. A more compact design is proposed below in order to reduce the manufacturing cost. The distance from the cavity to the HOM load is limited by the power absorption of the working mode. Consequently the main optimization parameter is the length of the HOM load. The design of HOM load using a different kind of material with higher losses (complex relative permittivity: 40+20j) was also investigated. However, no significant gain in the load length was obtained using more lossy materials.

The load with short length causes significant reflection of HOMs, which weakens the wakefield suppression. This reflection can be compensated by changing the geometry in the damping waveguide. Two ways of match the waveguide geometry to the reflection were proposed: Added a step on the side wall of the waveguide; or made a bended waveguide as shown in Fig. 18 Another potential advantage for the bended waveguides is reducing the amounts of manifolds from 4 to only 2. Both matching ways could achieve the compact cell design and the dimensions are shown in Fig. 18.

The wakefield results for both matching designs are shown in Fig. 19. Two different scales are plotted. The plot in Fig. 19 (a) is the wakefield value at the position of second following bunch (0.15 m). Due to the cancellation of the reflections from the stepped or the bended waveguide, the transverse wakefield kick amplitude at the position of the second bunch are smaller for both designs than the one with regular damping

waveguide. As shown in Fig. 19 (b), transverse wakefield kicks at some larger distance are higher for matching designs than the regular one. The overall wakefield suppression are still improved, which are seen by the numbers listed in Tab. 2.

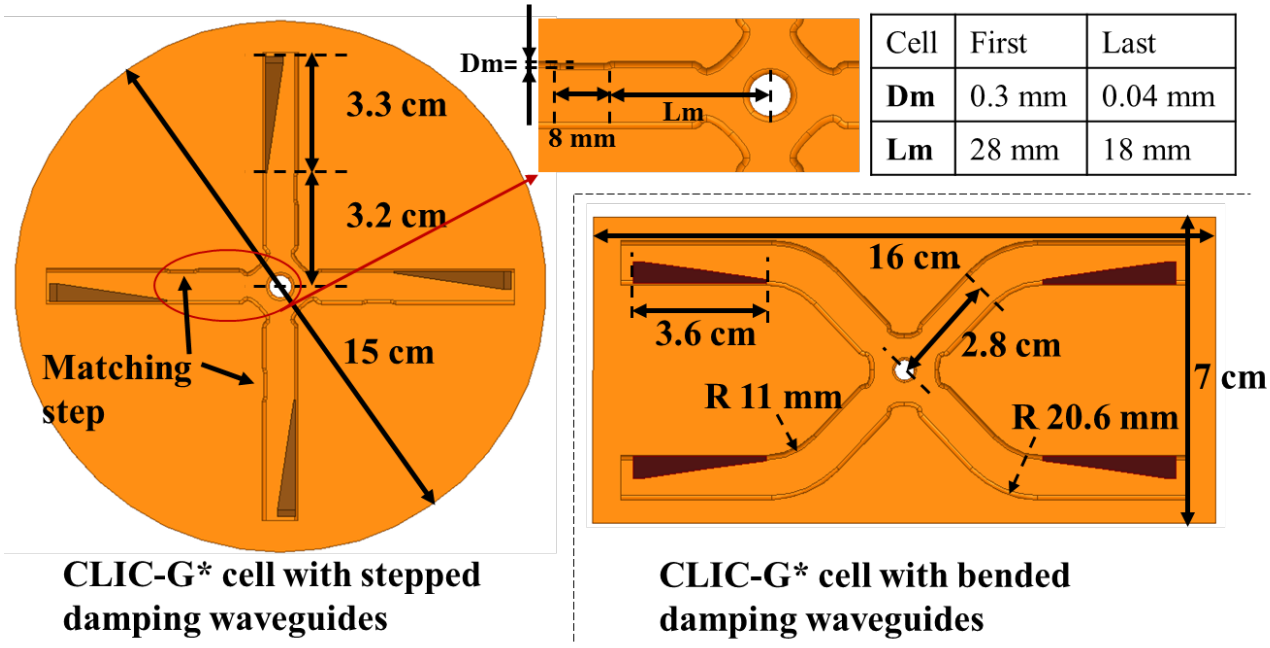

Cell	First	Last
Dm	0.3 mm	0.04 mm
Lm	28 mm	18 mm

Figure 18: Geometries of the HOM load designs for CLIC-G* structure with stepped damping waveguides and bended damping waveguides.

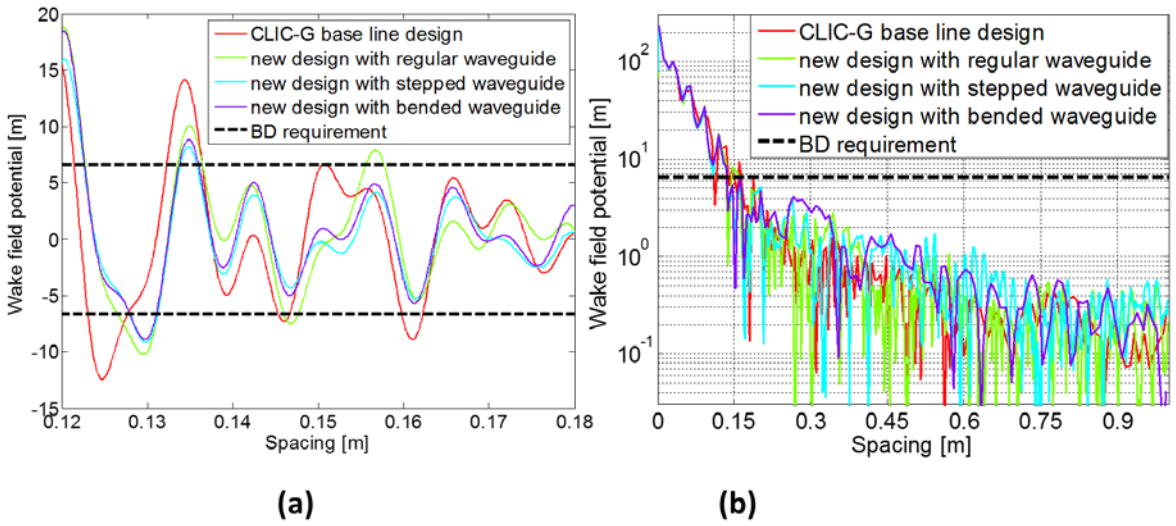

Figure 19: Wakefield of all designs in two difference scales: (a) wakefield at the nearby position of the second bunch; (b) log-scale wakefield plot from 0 to 1 meter.

Tab. 2: transverse beam jitter amplification factors in wakefield suppression of all structure designs.

Structure	CLIC-G base line	New CLIC-G regular waveguides	New CLIC-G stepped waveguides	New CLIC-G bend waveguides	Beam dynamics requirement
F_c	1.07	1.02	1.02	1.03	--
F_{rms}	3.9	1.1	1.2	1.5	< 5
F_{worst}	15.6	2.9	2.7	6.3	--

It is necessary to check the dependence of wakefield suppression on variation of the permittivity and the loss tangent of the SiC material, since material properties may vary from one manufacturing batch to another and measurements on material properties may be not accurate. Wakefield simulations results of new CLIC-G structure (regular waveguide) with the HOM loads with same geometries but various material properties are shown in Fig. 20. The wakefield suppression of the nominal design is already greatly improved, even after that material properties changed by 10% the wakefield suppression is still far better than requirements.

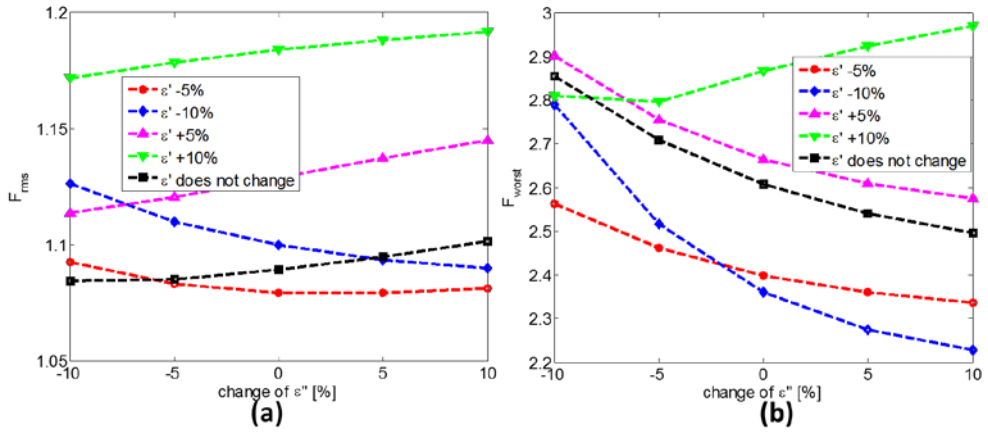

Figure 20: Wakefield suppression for RF loads with various material properties (ε': real part of permittivity, ε'': imaginary part of permittivity): (a) F_{rms}; (b) F_{worst}.

6. HOM free input power coupler

The geometry of input and output couplers are similar to those of regular cells, which use four damping waveguides to damp dipole modes in two polarizations. Unlike regular cells, two power coupling waveguide branches of input coupler are not terminated by HOM loads but rather by a power splitter (see Fig. 10 (b)). The excited dipolar wakefield in the input coupler will transmit through the coupling waveguide branches and will reach the power splitter. Fig. 22 (a) shows the simulated transverse wakefield in two cases: the power splitter fully absorbs all HOMs or reflects all HOMs. The discrepancy of wakefields in these two cases shows the amplitude of reflected transverse wakefield at the power splitter is at the level of 3 V/pC/m/mm. It causes non-negligible increase in F- factors. The suppression of this reflected wakefield is needed. A major dipole mode with the frequency of 17 GHz dominates the reflected wakefield, as shown in the wakefield spectrum in Fig. 22 (b). Consequently, a special design of the power splitter is needed to reduce its reflection of 17 GHz.

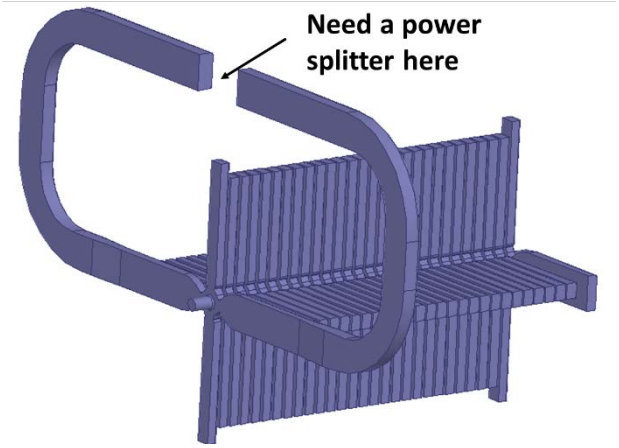

Figure 21: Power coupling circuit of CLIC accelerating structure.

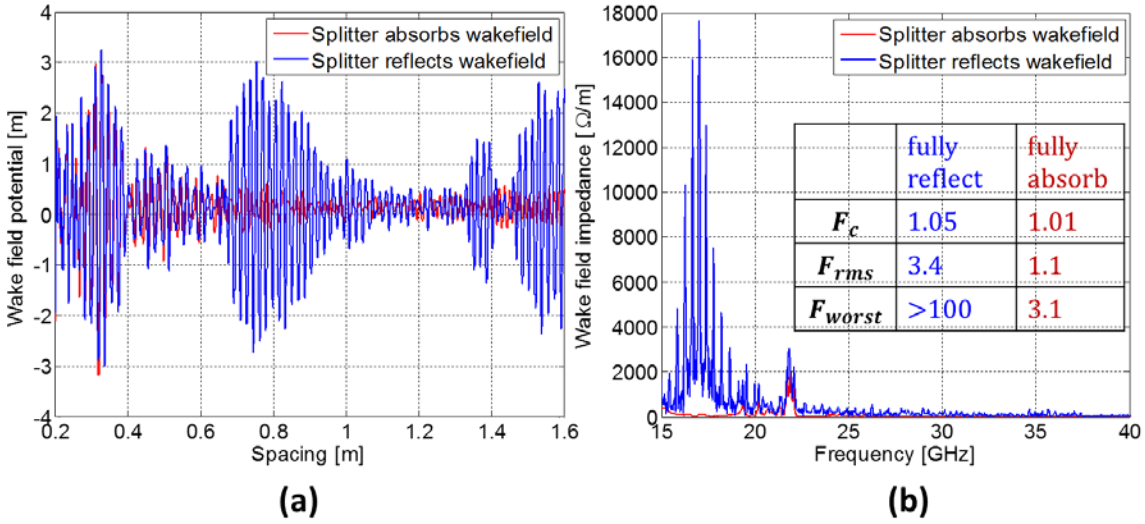

Figure 22: Transverse wakefield of new CLIC accelerating structure with splitter absorbing or reflecting the dipolar wakefield: (a) time-domain (please note the horizontal scale starts not from 0), (b) spectrum.

The suppression of dipole modes in the power splitter should be done in the similar manner as in the regular cell by absorbing dipole modes and, at same time, not affecting the fundamental mode. Furthermore, the power splitter should split the working frequency to two waveguide branches at same phases and absorb dipolar wakefields from two branches with 180 degree phase differences. Magic-T is the perfect solution to this requirement, as shown in Fig. 23. Ports #2 and #3 of the Magic-T are connected to two waveguide branches of the input coupler cell, port #1 is connected to the power source and port #4 is terminated by a HOM load to damp the dipolar wakefields.

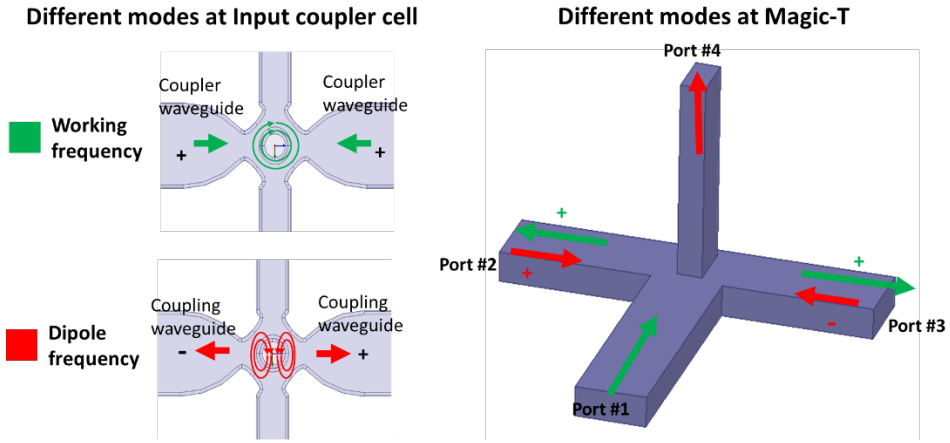

Figure 23: Power coupling and HOM damping in (a) the coupler cell and (b) the HOMagic-T.

The design of this HOMagic-T is difficult because the WR90 waveguide which is used here for transmitting X-band RF power allows multiple waveguide modes (TE_{10}, TE_{20}, TE_{01}, TE_{11}) of the major dipole band (17 GHz) to propagate. The final geometry design is shown in Fig. 24 after careful optimization. A step geometry in the central part of the Magic-T is used to reduce the mismatch of splitting the working frequency, which can improve the bandwidth of working frequency as well as reduce the maximum surface field (Peak surface electrical field = 37 MV/m for transmitting 61 MW power from port #1). There is a well-like shape in the bottom part of the Magic-T, which is used to keep the symmetry and avoid the TE_{02}-like propagating mode of the major dipole band. The step located between Magic-T and branch 1# is used to tune the frequency of trapped modes away from the major dipole band. Matching iris in the branch 1# is used to make a perfect

match for working frequency. Fig. 25 shows the HFSS simulation results, where sub-figure (a) shows the bandwidth of working frequency and sub-figure (b) shows the reflection of major dipole band.

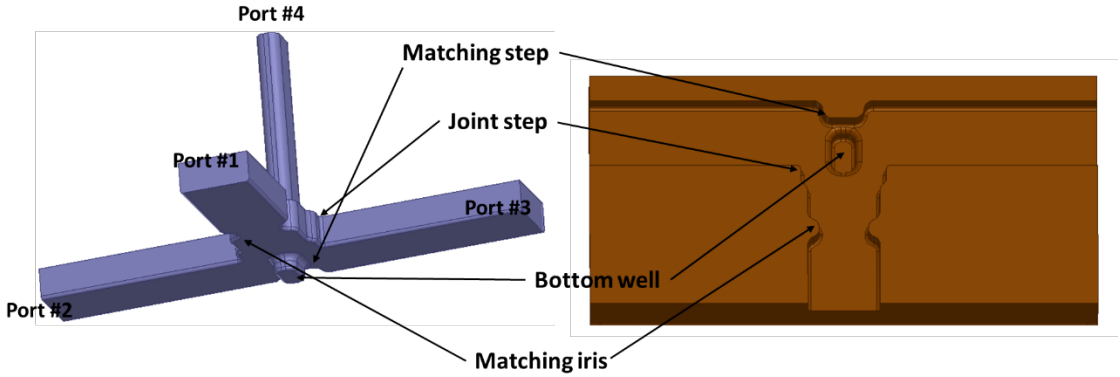

Figure 24: Geometry of the special HOMagic-T design.

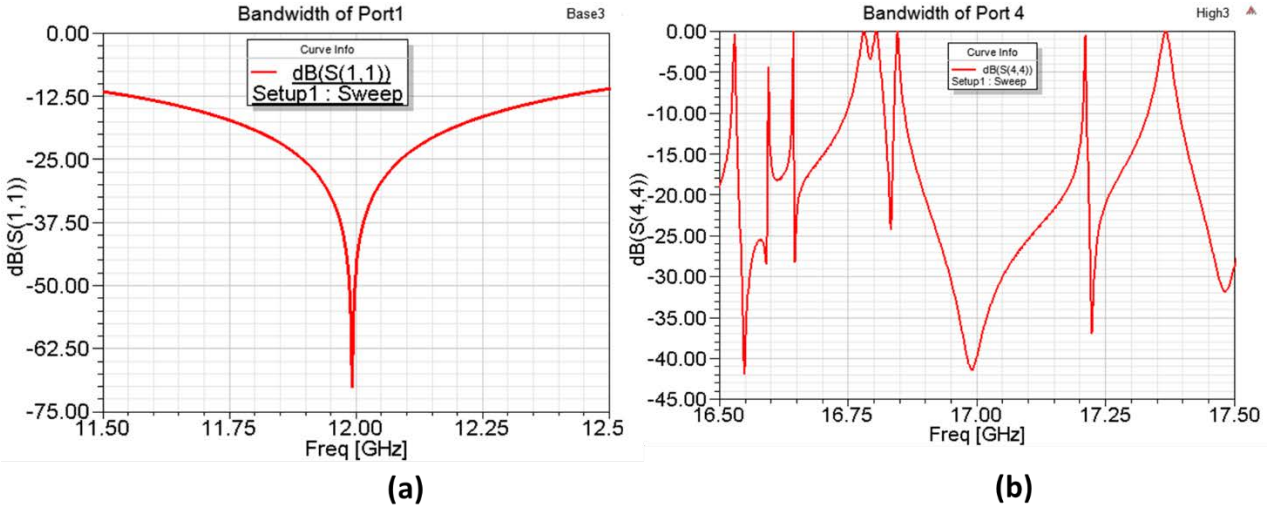

Figure 25: Bandwidth of (a) the working frequency and (b) the major dipole frequency in the Magic-T design.

Wakefield simulation results of the new CLIC-G structure with input coupler connecting this HOMagic-T design is shown in Fig. 26 and are compared to those of input coupler terminated by prefect matched layer (PML). Three F-factors of both cases are also listed and verified that this HOMagic-T design fit the wakefield suppression requirements.

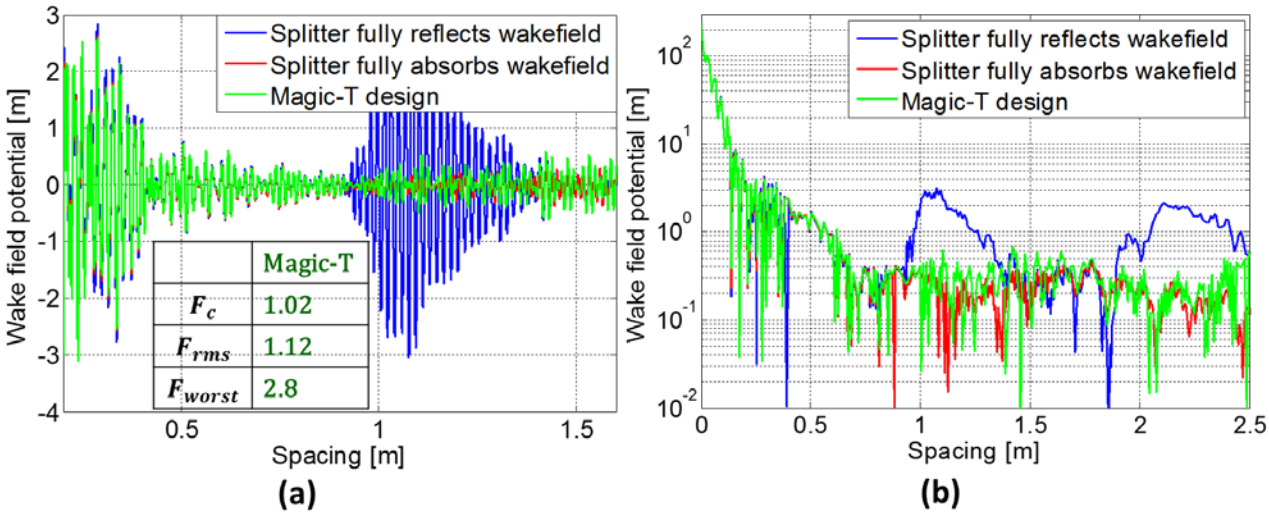

Figure 26: Wakefield of the new CLIC-G accelerating structure with the HOMagic-T design: (a) linear scale; (b) log scale.

7. Summary

Recent researches on the CLIC-G base line structure including high power tests, wakefield measurements and manufacturing studies have given the direction for further optimization on the CLIC-G structure geometry. A 4-th order polynomial shape was proposed for the wall profile of new CLIC-G structure cells instead of elliptical shape to reduce the surface magnetic field. We increased the rounding of structure cells from 0.5 mm to 1 mm, in order to reduce the total manufacturing cost. With the 1 mm rounding, we re-optimized the waveguide geometry (new waveguide width: 10.1 mm) to reduce the surface magnetic field. The waveguide geometry (opening) is set individually for each structure cell to avoid the appearance of hot cells in terms of pulse temperature rise. With all above improvements on the geometry employed, 10 K reduction of maximum pulse temperature rise, 7% reduction of the manufacturing cost and 1 MW reduction of the input power are achieved for the new CLIC-G structure design.

The geometry of HOM damped load for the new CLIC-G structure design was optimized to reduce transverse size of the structure. Other than a uniform damping waveguide, a new waveguide geometry with matching step and bended waveguide was proposed to further reduce the diameter. Wakefield suppression of the three proposed HOM load designs are verified by Gdfidl simulations and the results are even better than the old CLIC-G base line design.

A special power splitter using HOMagic-T geometry was designed for the double feed input coupler. This power splitter could absorb the major dipole band (17 GHz) excited in the coupler cell and meet the wakefield suppression requirements in the new CLIC-G design.

Acknowledgement

Authors are grateful to W. Wuensch for his constant support, useful comments and careful reading the manuscript.

Reference

[1] CLIC Conceptual Design Report (CDR), 2012, http://project-clic-cdr.web.cern.ch/project-CLICCDR/CDR_Volume1.pdf

[2] A. Grudiev, W.Wuensch, Design of the CLIC main linac accelerating structure for CLIC Conceptual Design Report. LINAC'10, Tsukuba, Japan, 2010.

[3] FACET facility in SLAC National Laboratory, http://portal.slac.stanford.edu/sites/ard_public/facet/Pages/default.aspx

[4] Hao Zha, Andrea Latina, Alexej Grudiev, Giovanni De Michele, Anastasiya Solodko Walter Wuensch, Daniel Schulte, Erik Adli, Nate Lipkowitz, and Gerald S. Yocky. "Beam-based measurements of long range transverse wakefields in CLIC main linac accelerating structure", Phys. Rev. Accel. Beams 19, 011001 (2016).

[5] W.Wuensch, Advances in the understanding of the physical processes of vacuum breakdown, Report No. OPEN-2014-028; Report No. CLIC-Note-1025, CERN, 2014.

[6] N. Catalan-Lasheras, A. Degiovanni, S. Doebert, W. Farabolini, J. Kovermann, G. McMonagle, S. Rey, I. Syratchev, L. Timeo, W. Wuensch, B. Woolley, and J. Tagg, Experience Operating an X-Band High-Power Test Stand at CERN, in Proceedings of International Particle Accelerator Conference IPAC14 (2014), pp. 2288–2290

[7] A. Degiovanni, S. Doebert, W. Farabolini, A. Grudiev, J. Kovermann, E. Montesinos, G. Riddone, I. Syratchev, R. Wegner, W. Wuensch, A. Solodko, and B. Woolley, High-Gradient Test Results from a CLIC Prototype Accelerating Structure: TD26CC, in Proceedings of the International Particle Accelerator Conference IPAC14 (2014), pp. 2285–2287.

[8] A. Degiovanni, W.Wuensch, Comparison of the conditioning of high gradient accelerating structures, Phy. Rev. Accel. Beams 19, 032001 (2016)

[9] T. Higo, T. Abe, Y. Arakida, S. Matsumoto, T. Shidara, M. Y. T. Takatomi, A. Grudiev, G. Riddone, and W. Wuensch, in Proceedings of the 4th International Particle Accelerator Conference, IPAC-2013, Shanghai, China, 2013 (JACoW, Shanghai, China, 2013), pp. 2741–2743

[10] S. Matsumoto, T. Abe, Y. Higashi, T. Higo, and Y. Du, Nucl. Instrum. Methods Phys. Res., Sect. A 657, 160 (2011).

[11] Walter Wuensch. High-gradient acceleration: CLIC and beyond. Talk in 2016, CLIC workshop, Geneva, Switzerland (2016).

[12] Said Atieh, private communication.

[13] A. Grudiev, S. Calatroni, and W. Wuensch. New local field quantity describing the high gradient limit of accelerating structures. Phys. Rev. ST Accel. Beams 12, 102001(2009).

[14] G. De Michele, "Wakefield Simulations and Measurements for the CLIC RF Accelerating Structure", Ph.D thesis, École Polytechnique Fédérale de Lausanne, 2014.

[15] D. Schulte, "Multi-bunch calculations in the CLIC main linac", in Proceedings of the 23rd Particle Accelerator Conference, Vancouver, Canada, 2009 (IEEE, Piscataway, NJ, 2009).